Computational Study on the Properties and Structure of Methyl Lactate

Santiago Aparicio*

Departamento de Química, Universidad de Burgos, 09001 Burgos, Spain

Received: January 31, 2007; In Final Form: March 22, 2007

A theoretical study on the properties and molecular level structure of the very important green solvent methyl lactate is carried out in the gas phase and methanol and water solutions, with the solvent treated both explicitly and as a continuum. Torsional barriers giving rise to different conformers by rotation of the hydroxyl and methyl groups were analyzed using density functional theory (DFT) to establish the most stable conformer both in gas phase and solution. DFT computations on lactate dimers were also done to study short-range features, and the effect of the surrounding solvent on intra- and intermolecular hydrogen bonding was analyzed according to the polarizable continuum model approach. We have also studied lactate/water and lactate/methanol small clusters together with the corresponding binding energies. Moreover, classical molecular dynamics simulations (MD) were carried out to study medium- and large-range effects at lower computational cost. MD simulations at different pressure and temperature conditions on pure lactate were carried out, and mixtures with water and methanol of different compositions were also studied. Structural information, analyzed through the radial distribution functions, together with dynamic aspects of pure and mixed fluids were considered. The intramolecular hydrogen bonding ability of methyl lactate together with the possibility of homo- and hetero-intermolecular association determines the behavior of this molecule in pure fluids or in mixed.

1. Introduction

Environmental regulations developed in the last few years all around the world responding to an increasing green sensibility in society have given rise to the growing and pressing need of preventing and/or reducing pollution at its source whenever feasible.[1] From an economical viewpoint, this would reduce related costs such as waste disposal or cleaning procedures[2] but also would decrease the associated risks of handling and manufacturing toxic, hazardous, and polluting materials. This is a great technological and scientific challenge[3] from a chemical viewpoint, requiring that chemistry and chemical engineering move toward a so-called green framework, giving rise to the development of new tools, chemical products, and/or processes, with pollution prevention as the central objective, establishing sustainable technologies, but also without losing efficiency or quality in the developed products, to minimize the environmental impact without stifling scientific progress. This green chemistry approach requires the use of innovative solutions to many real life or industrial problems but also requires a deep and wide knowledge of all the products and processes involved from the basis, to develop the most adequate solutions considering very different aspects, not only from a purely chemical viewpoint but also considering other viewpoints in the whole cycle of the chemical product such as human and environmental toxicology or biodegradability. One of the ubiquitous problems in almost any chemical process is the need for solvents, as most of the chemistry happens in solution. Solvents are used in a multiton scale, and in fact, one of the 12 principles proposed to develop a new paradigm in green chemistry requires the use of safer solvents.[1] These solvents used in the industry have very different characteristics and chemical natures, although most of them have an organic nature, but many of them produce severe effects on the environment not only at a local scale but also at a global one, considering that many of them are volatile organic compounds with strong atmospheric effects. Several approaches have been proposed to circumvent this problem;[4] the first and obvious one is to develop solvent-free processes. Although several applications have been developed within this framework,[5] the most realistic option at the moment is to substitute the highly polluting present solvents by environmentally friendly new ones together with the development of efforts for recycling and efficient use of these solvents.

Many different families of green solvents have been proposed in the last few years;[6] two of the most important ones are supercritical fluids and mainly ionic liquids. Although an enormous effort is being developed in the scientific community to study the properties and applications of these two alternative groups of solvents, other useful alternatives are also possible mainly arising from bio−derived sources. The lactate ester family is a group of compounds that are nontoxic and highly and readily biodegradable,[7] with excellent solvent properties that could replace toxic and environmentally unfriendly compounds.[8] Lactate esters may be obtained from carbohydrate feedstock, and the recent development of new purification processes based on selective membranes[9] has decreased their price remarkably, making technically and economically viable the use of lactate solvents for a wide range of industrial and consumer uses, replacing environment-damaging solvents including many volatile organic compounds and ozone depleting fluids.[10]

To develop efficient products and/or processes, the selection of adequate solvents is a key step in any process design. Thus, the replacement of a solvent by a new one requires the knowledge of its properties in the fluid state.[11] A useful approach to characterize any fluid is through the available molecular simulation tools that provide not only detailed information about the molecular level features but also allow the prediction of

* Corresponding author. E-mail: sapar@ubu.es.

10.1021/jp070841t CCC: $37.00
Published on Web 05/10/2007

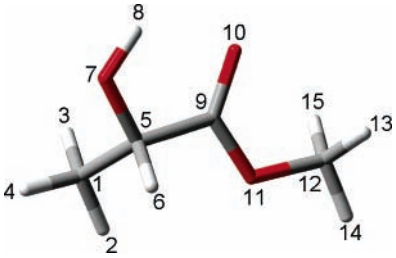

Figure 1. Optimized gas phase structure of ML1 computed at the B3LYP/6-311++g** theoretical level. Atom color code: gray = carbon, white = hydrogen, and red = oxygen.

macroscopic thermophysical properties, considering that the accurate experimental determination is difficult and economical and time-consuming, and then developing structure−property relationships.

The simplest member of the lactate ester family is methyl lactate, ML (Figure 1). It was studied in this work as a model to analyze the main features that determine the structure of this type of solvent in the liquid phase together with its intra- and intermolecular hydrogen bonding ability. As the S− enantiomer is the prevailing one, in this study, all the computations were performed for this isomer. Lactate esters are commonly produced by esterification of lactic acid with the corresponding alcohol, and thus, they are obtained in a mixture together with water and alcohol from which they have to be separated.[12] Thus, it is important to clarify the molecular−level structure of liquid lactate esters not only in the pure state but also in water and alcohol (methanol for ML) solutions. Density functional theory (DFT) computations were carried out in the gas phase and water and methanol solutions, using a polarizable continuum model (PCM). Intramolecular hydrogen bonding was established, and different conformations together with torsional profiles were studied. ML dimers and different ML + water or + methanol complexes were studied, and the interaction energies were computed. Classical molecular dynamics (MD) simulations were also carried out using an all-atom force field to include a larger number of molecules to study short- and long-range effects at a lower computational cost.

2. Computational Methods

2.1. DFT Computations. DFT calculations were carried out with the Gaussian 03 package,[13] using the Becke gradient corrected exchange functional[14] and the Lee−Yang−Parr correlation functional[15] with the three parameter (B3LYP)[16] method. To describe electrons far and near to the nuclei, it is important to use large and flexible basis sets; here, 6-311++g** was used. Atomic charges cannot unambiguously be determined because they are not experimentally available; thus, a large number of methods has been proposed. In this work, they were calculated to fit the electrostatic potential (ESP)[17] according to the Merz−Singh−Kollman (MK)[18a] scheme, and the fitting procedure was also constrained to reproduce the overall molecular dipole moment. Charges calculated using the MK scheme show a small dependence on the computational method and basis set employed,[18b] and thus, they are considered to be clearly superior to Mulliken Charges. The MK method applied using large basis sets and correlated methods as was done in this work leads to practically the same results as other ESP based charges such as ChelpG or Resp.[18b,c] These MK charges were used for MD simulations; ML is expected to be more polarized in solution than in the gas phase due to many interactions and thus Hartree−Fock (HF) derived charges, which used to be larger than B3LYP ones, probably were more suitable for liquid MD purposes. The basis set effect used to be larger than the HF or B3LYP effect; thus, we have decided for homogeneity purposes to use charges calculated at the B3LYP/6-311++g** level, which is a high theoretical level. The use of B3LYP derived charges is a common procedure in the literature that gives rise to reliable MD simulations.[18d−f] Solution calculations for monomers and complexes were carried out using the self-consistent reaction field approach (SCRF) with the solvent treated as a continuum using the integral equation formalism of the PCM approach (IEF−PCM).[19] The cavity in which the solute is placed in the IEF−PCM approach was built using the united atom model in all cases, and a value of 1.2 was used to scale all the radii and 70 tesserae to divide the spherical surfaces. All reported structures, conformers, and complexes were optimized in the gas phase, and then they were re-optimized inside the PCM cavity using the gas phase optimized ones as initial guesses. Vibrational frequencies were calculated at the same theoretical level of geometry optimizations, and the minimum energy geometries were determined to be true minima by the absence of imaginary frequencies in the calculated vibrational spectrum. Torsional barriers were calculated through relaxed scanning of the potential energy surfaces at 10° intervals; in this scanning procedure for each change of the corresponding torsional angle, the structure was fully optimized for the remaining degrees of freedom. The energy of the complexes was calculated as the difference among the complex and monomer energies with the basis set superposition error (BSSE) corrected according to the counterpoise procedure.[20]

2.2. Molecular Dynamics Simulations. Classical molecular dynamics simulations were carried out using the TINKER molecular modeling package.[21] All simulations were performed in the NPT ensemble; the Nosé−Hoover method[22] was used to control the temperature and pressure of the simulation system. The motion equations were solved using the Verlet Leapfrog integration algorithm.[23] Long-range electrostatic interactions were treated with the smooth particle mesh Ewald method.[24] The simulated systems consisted of cubic boxes with 250 total molecules to which periodic boundary conditions were applied in the three directions to simulate an infinite system. The initial liquid box sizes were established according to the experimental densities when available, whereas for mixtures, ideality was supposed. The simulations were performed using a cutoff radius of $L/2$ Å for the nonbonded interactions, L being the initial box side. Initial boxes generated using the PACKMOL program[25] were minimized according to the MINIMIZE program in the TINKER package to a 0.01 kcal mol^{-1} $Å^{-1}$ rms gradient, and then several heating and quenching steps in the NVT ensemble up to 500 K were performed, after which a 100 ps NVT equilibration molecular dynamics simulation was run at the studied temperature; finally, from the output NVT simulation configuration, a run of 500 ps (time step 1 fs) in the NPT ensemble at the studied pressure and temperature was run, from which the first 100 ps was used to ensure equilibration (checked through constant energy) and the remaining 400 ps for data collection. ML was described according to the so-called optimized potential for liquid simulations (all-atom version) OPLS-AA.[26] This model has been applied successfully to compute liquid state properties for different systems.[27] MK charges obtained through the B3LYP/6-311++g** calculations were used in the simulations. Methanol was also simulated according to the OPLS-AA forcefield, with charges obtained from Jorgensen et al.,[26] whereas water was studied according to the simple point charge model (SPC),[28] which performs reasonably well in reproducing the structural and thermodynamic

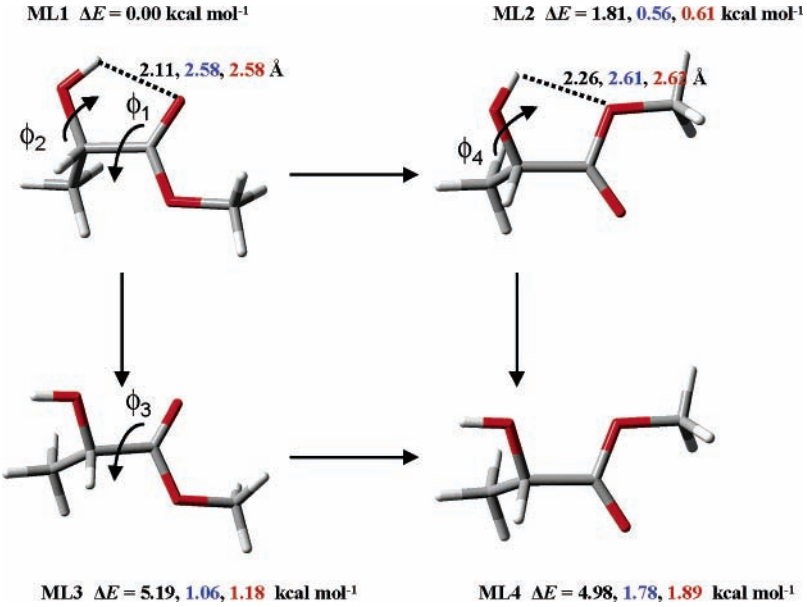

Figure 2. Optimized gas phase structures of the four most stable conformers of ML (ML1−ML4) computed at the B3LYP/6-311++g** theoretical level. Atom color code as in Figure 1. ΔE is the energy relative to the conformer with lower energy (ML1). ΔE and hydrogen bonding distances reported for gas phase (black), IEF−PCM water (blue), and IEF−PCM methanol (red) solutions. Scanned dihedral angles: (a) ϕ_1 (7−5−9−10) (ML1 to ML2), (b) ϕ_2 (8−7−5−9) (ML1 to ML3), (c) ϕ_3 (7−5−9−10) (ML3 to ML4), and (d) ϕ_4 (8−7−5−9) (ML2 to ML4). Atom numbering as in Figure 1.

properties and the dynamics of water.[29] In spite of the simplicity of the SPC water model, it has been applied in this work together with the B3LYP/6-311++g** MK derived charges for ML. This theoretical approach for ML is more complex than the one used for water, but it has been applied successfully for other complex systems in the literature.[29e]

3. Results and Discussion

3.1. DFT Computations. The study carried out at the B3LYP/6-311++g** theoretical level allows us to infer information about the ML monomer structure but also allows us to analyze the energy and stability of the ML complexes formed by auto- or heteroassociation through hydrogen bonding, either in the gas phase or in the water and methanol solutions. This DFT study allows us to analyze short-range effects in a highly accurate fashion.

3.1.1. ML Monomer. As mentioned previously, the S optical isomer of ML prevails, and thus, this is the enantiomer considered in this work. The relative position of the hydrogen pertaining to the hydroxyl group relative to the oxygens in the ester group determines the ability of intramolecular hydrogen bonding formation but also which ester oxygen, carbonyl or alkoxy, in the vicinity of the hydroxyl group contributes to the relative stability of the different conformers. Thus, four different main conformers are possible, ML1−ML4, that may be obtained through the rotation of different dihedrals, ϕ_1−ϕ_4 (Figure 2). Conformers ML1 and ML2 allow the formation of intramolecular hydrogen bonding with the carbonyl and alkoxy oxygens, respectively, whereas for ML3 and ML4, intramolecular hydrogen bonding is not possible. The order of stability is ML1 > ML2 > ML3 > ML4 (except for the gas phase in which ML4 has a slightly lower energy than ML3). If we compare the energies obtained for ML3 and ML4, in which hydrogen bonding is absent (the energy differences among both conformers is produced by the relative position of the ester oxygens and the hydroxyl group), we may conclude that more stable structures are obtained with the carbonyl group eclipsing the hydroxyl group, except for the gas phase in which the alkoxy oxygen eclipsing the hydroxyl group is slightly favored (0.21 kcal mol^{-1}); however, the energy difference among both conformers is very small (0.72 and 0.71 kcal mol^{-1} in water and methanol solutions, respectively). ML1 is the most stable conformer both in the gas phase and in the water and methanol solutions, and the hydrogen bond with the carbonyl oxygen in ML1 is clearly stronger than the one with the alkoxy oxygen in ML2 in the gas phase (5.19 kcal mol^{-1} for ML1 and 3.17 kcal mol^{-1} for ML2), but in the water and methanol solutions, the strength of the hydrogen bonding is slightly greater in ML2 (1.22−1.28 kcal mol^{-1} for ML2 and 1.06−1.18 kcal mol^{-1} for ML1 in water and methanol, respectively). ML1 shows a slightly lower energy than ML2 because of the aforementioned stability factor obtained by the carbonyl oxygen eclipsing the hydroxyl group. Thus, the energy differences among the conformers decreases remarkably on going from gas to water or methanol solutions with the strength of the hydrogen bonding decreasing both for ML1 and for ML2. This is confirmed by the longer distance among the hydrogen and oxygen in both conformers that should weaken the hydrogen bonding. This is produced because in the gas phase, the dihedral angles (9−5−7−8) and (7−5−9−10), which show the position of the hydroxyl hydrogen relative to the carbonyl oxygen and the eclipsing position of the hydroxyl and oxygen in the ester groups, move from values close to zero in the gas phase to a clearly out-of-plane position (Table S1, Supporting Information), thus weakening the hydrogen bond. These gas phase results are in agreement with literature computations developed at different theoretical levels,[30,31] but no previous PCM studies could be found to allow for a comparison. Considering the relative energies of the four conformers reported in Figure 2, the populations can be calculated considering a Boltzmann distribution at 298.15 K; thus, (95.5, 4.5, 0.0, and 0.0%) in the gas phase, (62.3, 24.2, 10.4, and 3.1%) in IEF−PCM water, and (65.1, 23.3, 8.9, and 2.7%) in IEF−PCM methanol for ML1−ML4 are obtained. These populations show that although in the gas phase ML1 is predominant and ML3−ML4 are almost absent, in the water and methanol solutions, the populations of conformers without

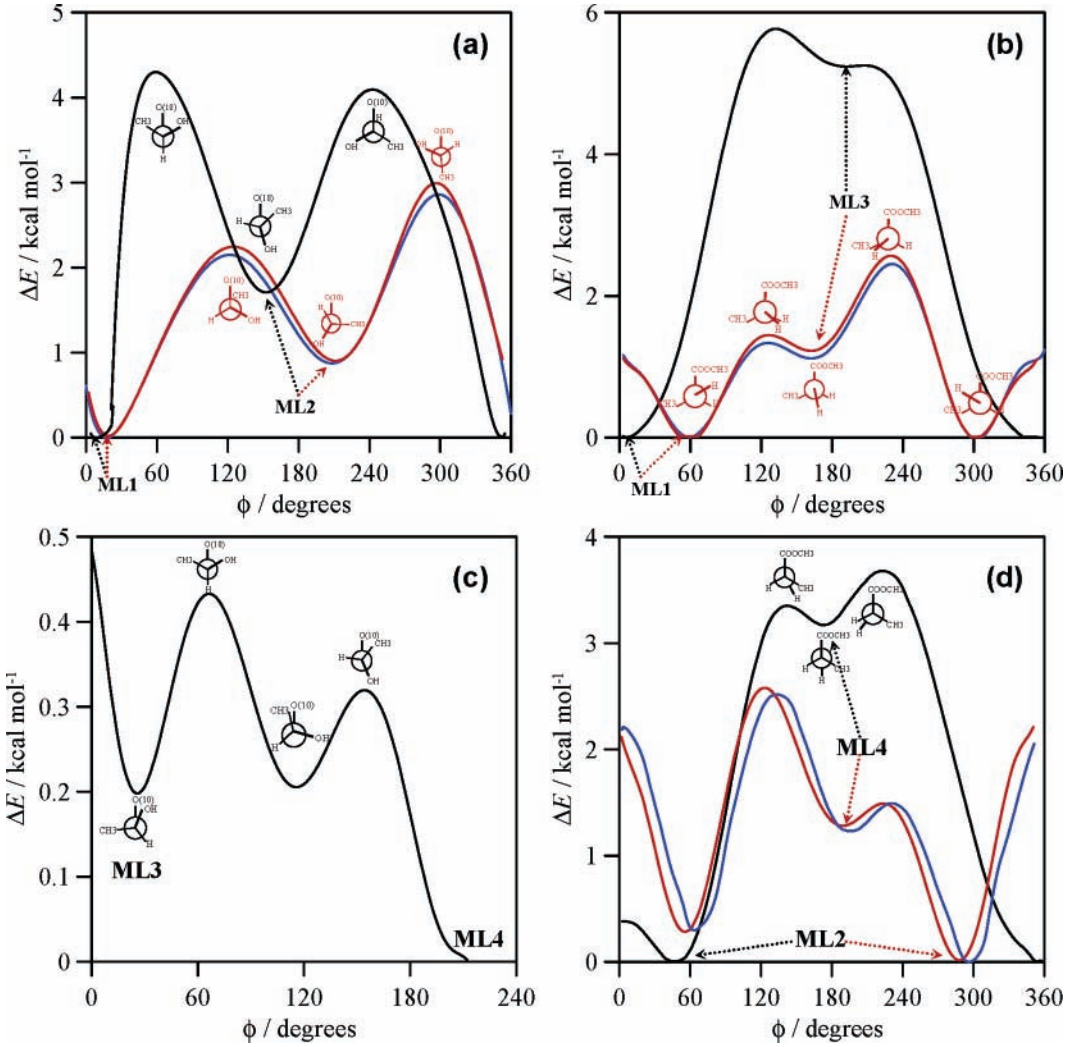

Figure 3. Relaxed potential energy scans computed at B3LYP/6-311++g** theoretical level for ML in gas phase (black), IEF−PCM water (blue), and IEF−PCM methanol (red) solutions. Scanned dihedral angles as in Figure 2. Δ*E* is the energy relative to the conformer with lower energy for each scan (ML1 for panels a and b, ML4 for panel c, and ML2 for panel d). Newman projections plotted along the 5−9 bond for panels a and c and 7−5 for panels b and d.

the ability of forming intramolecular hydrogen bonding increase, showing the effect of competing intermolecular hydrogen bonding with the surrounding water/methanol medium that weakens the intramolecular interaction in spite of the fact that in the PCM approach the solvent molecules are not treated explicitly.

Potential energy scans for several important dihedrals are reported in Figures 3 and 4. Rotation around the (7−5−9−10) dihedral allows the conversion from ML1 to ML2. This conversion evolves in the gas phase through a transition state of high energy (Figure 3a); thus, this barrier cannot be surpassed at ambient temperature conditions. This rotational barrier is decreased on going from the gas to water/methanol solutions and also the transition states are different; however, the torsional profiles are almost the same for water and methanol solutions, and transition states are stabilized by the surrounding solvent. The rotation around the (8−7−5−9) dihedral to evolve from ML1 to ML3 shows the strength of the (O)H−O(=C) intramolecular bonding (Figure 3b), and a great barrier is obtained with the energy of the transition states decreased to almost one-third on going to solutions; thus, remarkable populations of the ML3 conformer may be present in solution because of the competing intermolecular hydrogen bonding with water/methanol molecules. Evolution from ML2 to ML4 goes though a lower barrier, pointing to the weaker character of the hydrogen bond with the alkoxy oxygen. As for ML1, in solution, a certain number of molecules could evolve to the ML4 conformer through the low transition states reported (Figure 3d). The interconversion of the ML3−ML4 conformers was studied only in the gas phase (Figure 3c) because in the water/methanol solutions, ML3 evolves during the potential energy scanning procedure to ML1 instead of ML4. Low barriers are obtained, and thus, although the configuration in which OH and CO are eclipsed is preferred, it could evolve to ML4 at ambient temperature. We can also observe in Figure 3c a fifth conformer in the gas phase in which the methyl and carbonyl oxygen are eclipsed with energy only slightly greater than ML3. The absence of intramolecular bonding ability gives rise to an almost free rotation on going from ML3 to ML4. Thus, although the gas phase results point to a clearly prevailing ML1 configuration,[31−33] results in solution show that (i) intramolecular hydrogen bonds are weakened and (ii) remarkable populations of remaining isomers appear as a consequence of the weakening that increases the conformational flexibility of the molecule.

Torsional profiles for the rotation of the two methyl groups were also calculated for the ML1 conformer (Figure 4). Although for both groups the conformations at 60° are clearly favored, for the ester methyl group, the rotation evolves through

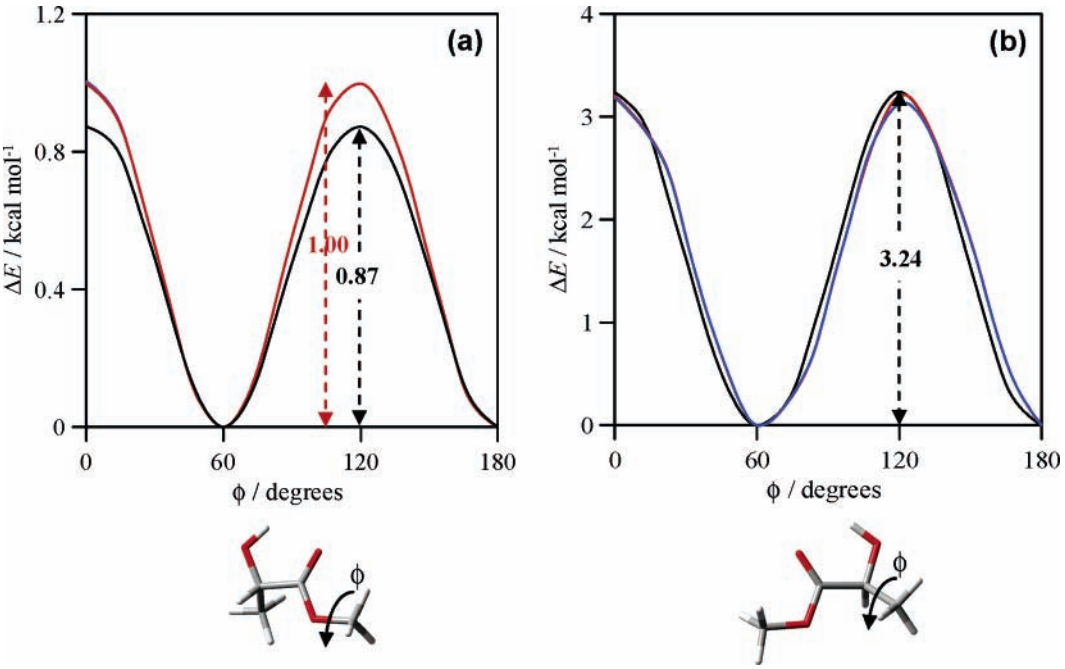

Figure 4. Computed relaxed potential energy scan for the reported dihedral angles in ML1 at the B3LYP/6-311++g** theoretical level. Atom color code as in Figure 1. Gas phase (black), IEF−PCM water (blue), and IEF−PCM methanol (red). Δ*E* is the energy relative to the conformer with lower energy for each scan.

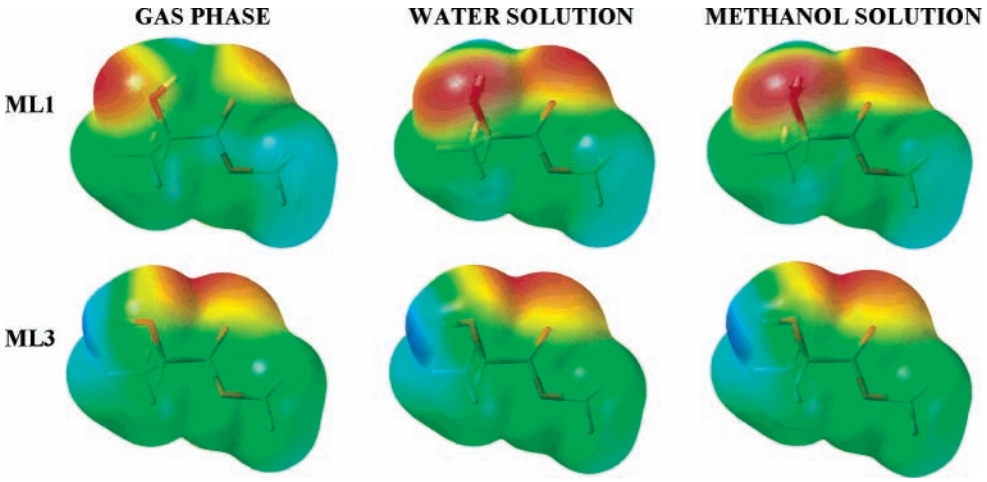

Figure 5. ML1 and ML3 electrostatic potential mapped on an electronic density surface isovalue of 0.0005 au calculated at the B3LYP/6-311++g** theoretical level in the gas phase and water and methanol (IEF−PCM) solutions. Atom color code as in Figure 1. Color scale for electrostatic potential: negative = red and positive = blue.

a low energy transition state that is almost unaffected by the surrounding media, and thus, free rotation is allowed for this group, whereas for the terminal methyl group, a remarkable barrier is obtained. This remarkable barrier can be related to the intramolecular interaction among the oxygen in the hydroxyl group and the hydrogen in the neighbor methyl group, and with a negligible effect of the surrounding solvent, this fact would have an effect on the solvation of this methyl group.

The electrostatic potentials for some conformers are reported in Figure 5. For conformers forming intramolecular hydrogen bonding, remarkable changes arise on going from the gas phase to solutions in the hydroxyl−carbonyl moieties; for the conformers without that ability, very small changes appear in those groups. For ML1, two separate zones of negative electrostatic potential around the hydroxyl and carbonyl oxygen appear in the gas phase, but in the water/methanol solutions, the movement of the hydroxylic hydrogen out of the plane gives rise to a continuous negative zone overlapping the hydroxyl and carbonyl groups; thus, intermolecular hydrogen bonding with the surrounding water/methanol molecules can be established in that position weakening the intramolecular hydrogen bonding. For ML3, as for ML4, the most remarkable changes appear in the positive zone close to the hydroxylic hydrogen that is reinforced in solutions. The calculated dipole moments are reported in Table 1. The order is always ML3 > ML1 > ML2 > ML4, and these dipole moments increase on going to the water/methanol solutions (except for ML2, which decreases slightly

TABLE 1: Dipole Moments (*μ*/D) of ML Conformers Calculated at B3LYP/6-311++g Theoretical Level in Gas Phase and Water and Methanol Solutions (IEF−PCM)**

	gas	water	methanol	$\mu_{water}-\mu_{gas}$	$\mu_{methanol}-\mu_{gas}$
ML1	3.129	3.402	3.362	0.273	0.233
ML2	2.533	2.549	2.483	0.016	−0.050
ML3	3.410	4.839	4.777	1.429	1.367
ML4	1.908	2.102	2.067	0.194	0.159

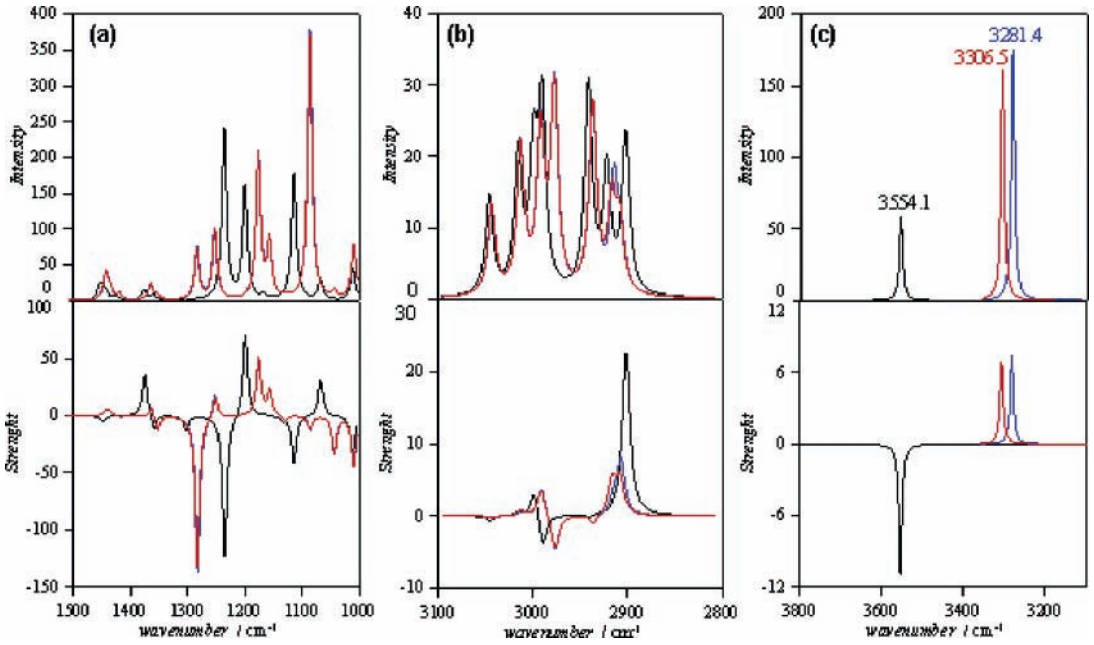

Figure 6. B3LYP/6-311++g** computed IR and VCD spectra of ML1 in (black) gas phase, (blue) IEF−PCM water, and (red) IEF−PCM methanol solutions. Harmonic wavenumbers scaled with a factor 0.96.

in methanol) with the stronger effects on ML1 and ML3. This is clearly related to the increasing negative zones in ML1 and the positive ones in ML3 in the solutions.

The use of the SCRF method allows for the calculation of solvation free energies, ΔG^{SOL}, of ML conformers in the water/methanol solutions. According to this well-known methodology, ΔG^{SOL} can be split into electrostatic and nonelectrostatic contributions

$$\Delta G^{SOL} = \Delta G^{ELEC} + \Delta G^{NONELEC} \quad (1)$$

where the nonelectrostatic term includes cavity, dispersion, and repulsion contributions

$$\Delta G^{NONELEC} = \Delta G^{CAV} + \Delta G^{DIS} + \Delta G^{REP} \quad (2)$$

The electrostatic contribution arises from the interaction between the solute charge distribution and the polarized solvent electric field (reaction field). The cavity term is the work needed to build the cavity in which the solute molecules are placed, the dispersion contribution arises from the London attractive forces, and the usually small repulsive term comes from the quantum exchange−repulsive interaction among the solute and the surrounding solvent. Table 2 summarizes the free energies of solvation together with the changes in energy when passing from the gas phase to the water/methanol solutions. The four conformers decrease in energy in solution in the order ML3 > ML4 > ML2 > ML1, indicating a very favorable interaction with the surrounding solvents conferring a great stability to the molecules. Conformers ML3 and ML4 are remarkably more stabilized in water/methanol solutions than ML1 or ML2, and this is produced because in these last conformers, a competition among intra- and intermolecular hydrogen bonding is established. Thus, the interaction with the surrounding solvent is less effective than in ML3/ML4 for which the hydroxyl and carbonyl groups are free to establish intermolecular hydrogen bonds with the water/methanol solvents. The solvation energies reported in Table 2 show efficient solvation for the four conformers in the same order of ΔE; the larger the ΔE, the better the solvation. However, ML conformers are remarkably better solvated in methanol than in water solutions, as is shown by the almost double values of solvation free energies. This is in contrast to the almost equal values of ΔE for both solvents, and this fact arises from the lower values of the nonelectrostatic contributions to the total free energies of solvation that are almost half in the methanol solutions because of the larger cavitation energies in the water than in the methanol solutions. Considering the remarkable efficient solvation of the four conformers in the

TABLE 2: Changes of Energy ($\Delta E = E_{solution} - E_{gas}$), Free Energies of Solvation (ΔG_{sol}), and Electrostatic (ΔG_{elec}) and Nonelectrostatic ($\Delta G_{nonelec}$) Contributions to the ΔG_{sol} Calculated at B3LYP/6-311++g Theoretical Level in Water and Methanol Solutions (IEF−PCM) for ML Conformers[a]**

	ΔE	ΔG_{elec}	$\Delta G_{non-elec}$	ΔG_{sol}
ML1	−8.71	−10.17	8.82	−1.35
	−8.22	**−9.63**	**4.64**	**−4.99**
ML2	−9.96	−11.26	8.68	−2.58
	−9.42	**−10.73**	**4.54**	**−6.19**
ML3	−12.84	−13.39	8.67	−4.72
	−12.23	**−12.75**	**4.52**	**−8.23**
ML4	−11.90	−12.38	8.72	−3.66
	−11.31	**−11.78**	**4.56**	**−7.22**

[a] All energies in kcal mol^{-1}. Values in bold correspond to methanol solutions.

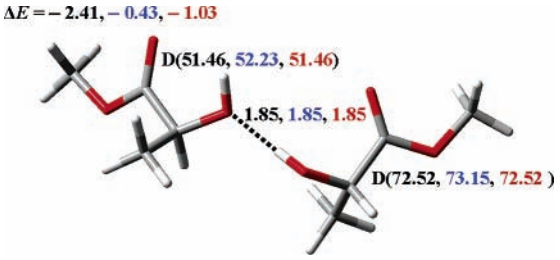

Figure 7. Highest binding energy ML dimers calculated at the B3LYP/6-311++g** theoretical level in the gas phase (black), water (blue), and methanol (red) (IEF−PCM) solutions. Atom color code as in Figure 1. Distances in angstroms, counterpoise corrected binding energies (ΔE) in kcal mol^{-1}. Dihedral angles reported (D) correspond to D(8−7−5−9) with ML numbering as in Figure 1.

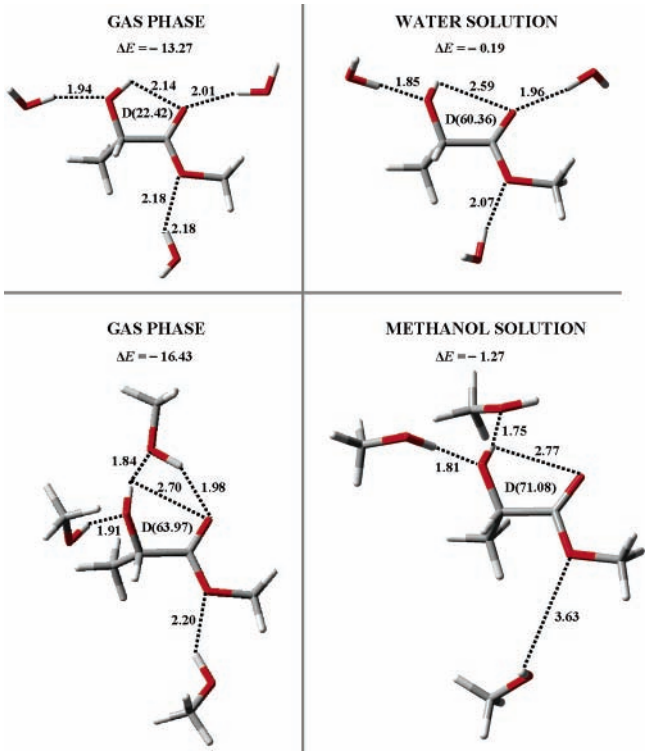

Figure 8. Highest binding energy ML1 + (three water or three methanol) complexes calculated at the B3LYP/6-311++g** theoretical level in the gas phase and water and methanol (IEF−PCM) solutions. Atom color code as in Figure 1. Distances in angstroms, counterpoise corrected binding energies (ΔE) in kcal mol^{-1}. Dihedral angles reported (D) correspond to D(8−7−5−9) with ML numbering as in Figure 1.

water and methanol solutions, the population ratios of the four conformers will change in the solutions, and significant quantities of ML2 but also of the ML3−ML4 conformers, without ability of intramolecular hydrogen bonding, will arise. Thus, the competing intra-−/intermolecular hydrogen bonding will increase the molecular flexibility of ML.

Infrared (IR) and vibrational circular dicroism (VCD) spectra were also calculated for ML1 in the gas phase and the water/methanol solutions. In Figure 6, results for the mid-IR, CH, and OH stretching regions are reported. Results in the gas phase are in agreement with literature experimental data and with values calculated at different theoretical levels.[30,31] Comparison with experimental gas phase spectra show that ML1 is the prevailing conformer in the gas phase, but remarkable changes in the ML1 spectra appear on going to solutions mainly in the OH− stretching region. A red shift in the IR and VCD spectra for the OH stretching region may be observed in Figure 6c, a clear sign of the weakening in the intramolecular hydrogen bonding, but also a change from the negative VCD in the gas phase to a positive one in the water/methanol solutions. This fact arises from the remarkable changes arising in the OH bond environment in solution. The hydroxyl hydrogen is placed out-of-plane in the water/methanol solutions, and then a positive feature appears in the VCD spectra. Hence, although several spectroscopic experimental[30−33] studies have been reported in the literature on the ML gas phase structure, those studied should be extended with caution when solution behavior is considered because of the remarkable changes that arise.

3.1.2. ML Clusters. The nature of short-range interactions is analyzed by the study of geometrical and energetical properties of several complexes established by self-association among ML molecules and by heteroassociation with water/methanol molecules. First, ML clusters were analyzed exploring different initial configurations. Experimental and theoretical studies have shown that up to tetrameric cyclic clusters are possible in the gas phase for ML through cooperative OH−OH bonding.[32−34] Considering that it is very difficult for these highly organized clusters to persist in water/methanol solutions because of the competition with hydrogen bonding with solvent molecules, we have studied only ML dimers. Dimers may be formed through carbonyl−hydroxyl interactions, giving arise to cyclic

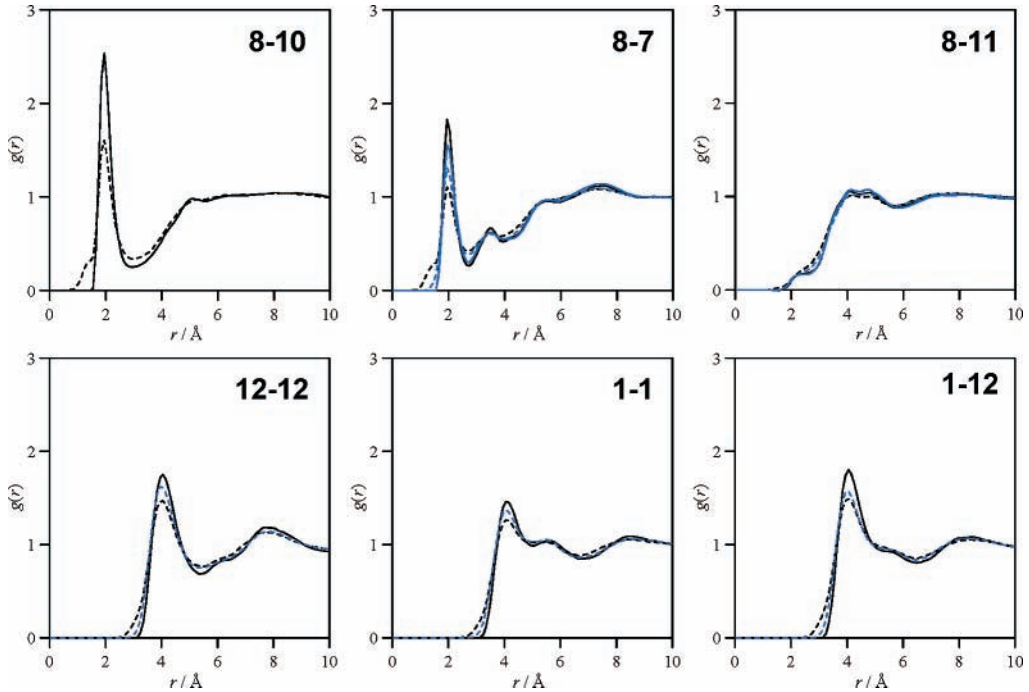

Figure 9. Site−site radial distribution functions, $g(r)$, for ML calculated from molecular dynamics simulations. (—) 298 K, 0.1 MPa; (---) 373 K, 0.1 MPa; (—, blue) 298 K, 50 MPa; and (---, blue) 373 K, 50 MPa. Atom numbering as in Figure 1. In some panels, $g(r)$ values at 50 MPa are omitted because they are almost equal to those at 0.1 MPa.

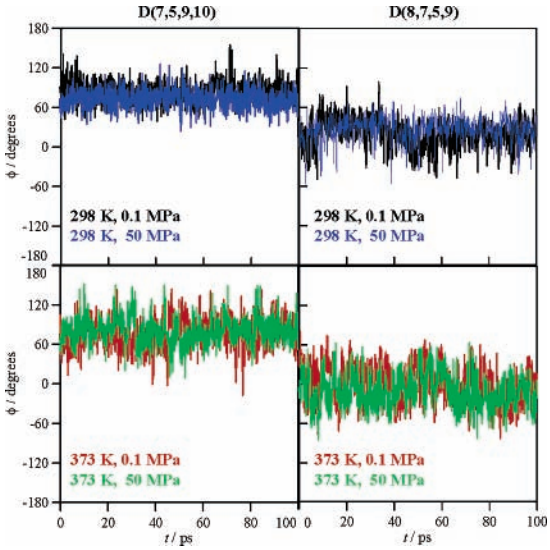

Figure 10. Time evolution of the selected dihedral angles, *D*, in ML for the last 100 ps of the molecular dynamics simulations at the reported temperatures and pressures. Atom numbering as in Figure 1.

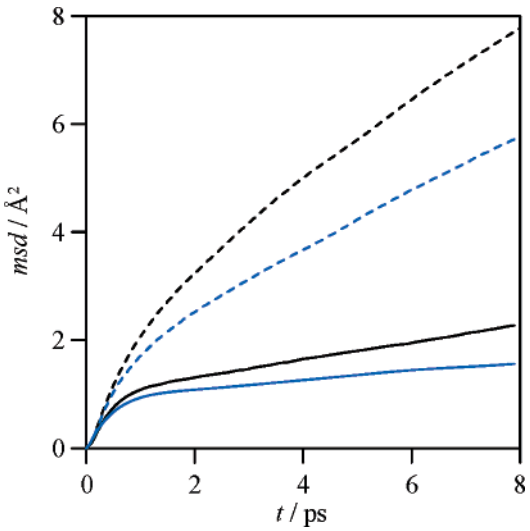

Figure 11. Mean square displacement, msd, for ML obtained from molecular dynamics simulations at different temperatures and pressures. Colors as in Figure 9.

8-ring clusters in which intramolecular hydrogen bonds disappear or through hydroxyl−hydroxyl heteroassociation in which the hydroxyl group of a molecule is inserted into the intramolecular hydrogen bond of a second molecule, allowing a certain degree of intramolecular hydrogen bonding.[32] Previous results[32] have shown that in the gas phase, the 8-ring clusters are slightly more stable (∼1.2 kcal mol^{-1}), but results reported in this work for the water/methanol solution show that in solution, the dimers formed by OH−OH interactions are the most favorable ones (Figure 7). The stability of the dimers decreases on going to water/methanol solutions; thus, a strong effect of the surrounding solvent on the ML self-association is also established, and hence, in solution, not only the intramolecular hydrogen bonds are weakened but also the intermolecular bonds among ML molecules because of the competition with the heteroassociation with the surrounding water/methanol molecules.

ML + (water or methanol) clusters were also studied to analyze the way in which these molecules form heteroassociations with ML, that is to say, through addition or insertion

TABLE 3: Properties of ML Computed from Molecular Dynamics Simulations[a]

T (K) − P (MPa)	ρ (g cm^{-3})	E_{int} (kcal mol^{-1})	c (MPa)	10^9 D (m^2 s^{-1})
298 − 0.1	1.1029	−15.77	699.56	0.18
	1.0898[b]			
	1.0873[c]			
298 − 50	1.1229	−16.18	730.10	0.09
373 − 0.1	1.0230	−13.56	557.75	0.87
373 − 50	1.0532	−14.03	594.47	0.56

[a] Density, ρ; intermolecular energy, E_{int}; cohesive energy density, c (calculated as $c = (-E_{int}/V_m)$); and diffusion coefficient, D (calculated from msd). [b] Reference 36. [c] Reference 37.

complexes.[35] No experimental or theoretical data have been found for ML/water, clusters but a study[35] on ML/methanol clusters has shown that for a one ML/one methanol cluster, insertion of an alcohol molecule within the ML intermolecular hydrogen bond is clearly favored. To analyze the solvation of ML by water/methanol molecules, clusters involving three solvent molecules in the three ML available sites were studied in this work in the gas phase and in water or methanol solutions (Figure 8). The results shows that one ML/three water/methanol complexes are very stable in the gas phase as is shown by the high binding energies. Water complexes show lower binding energies than methanol ones, but the stability of these complexes decreases remarkably on going to water/methanol solutions. Whereas for water complexes the addition complexes are preferred for methanol ones, insertion in the OH−O(=C) bond is preferred, as the intramolecular ML hydrogen bond is weakened for both solutions. For water complexes, a simultaneous interaction in the three sites of ML is possible, but for methanol in solution, the interaction with the alkoxy oxygen is very weak.

Hence, a very complex behavior of ML in solution may be expected from the short-range studies carried out at the DFT level, as several relevant conclusions may be inferred: (i) intramolecular hydrogen bonding in ML is strongly weakened in solution; (ii) self-association among ML molecules is also weakened in solution, nevertheless OH−OH interactions are favored; and (iii) interaction with methanol molecules is more favorable than with water ones, and the interaction with both molecules is weak in both solutions. Thus, a very delicate balance among intramolecular and intermolecular, homo and hetero, hydrogen bonding will determine the ML solution structure.

3.2. Molecular Dynamics Simulations. The study of medium- and long-range effects on the ML solution structure is carried out through classical molecular dynamics simulations. The properties of pure ML were studied as a function of pressure and temperature together with ML/water and ML/methanol binary mixtures at 298 K and 0.1 MPa as a function of composition. Finally, an equimolar ML/water/methanol ternary mixture was analyzed to study the whole solvation behavior of this system when the three considered molecules were present simultaneously.

3.2.1. Pure ML. As mentioned previously, the interaction among ML molecules could be established in three different ways: (i) OH−O(=C), 8−10; (ii) OH−OH, 8−7; and (iii) OH−O (alkoxy), 8−11. Although the DFT study has shown that interaction 8−7 is preferred, we are going to analyze this fact through molecular dynamics. Simulations of pure ML were carried out at 298 K, 0.1 MPa and 373 K, 0.1 MPa to study the temperature effect on ML structure and properties and at 298 K, 50 MPa and 373 K, 50 MPa to analyze the pressure effect. In Figure 9, we report radial distribution functions, RDFs, for

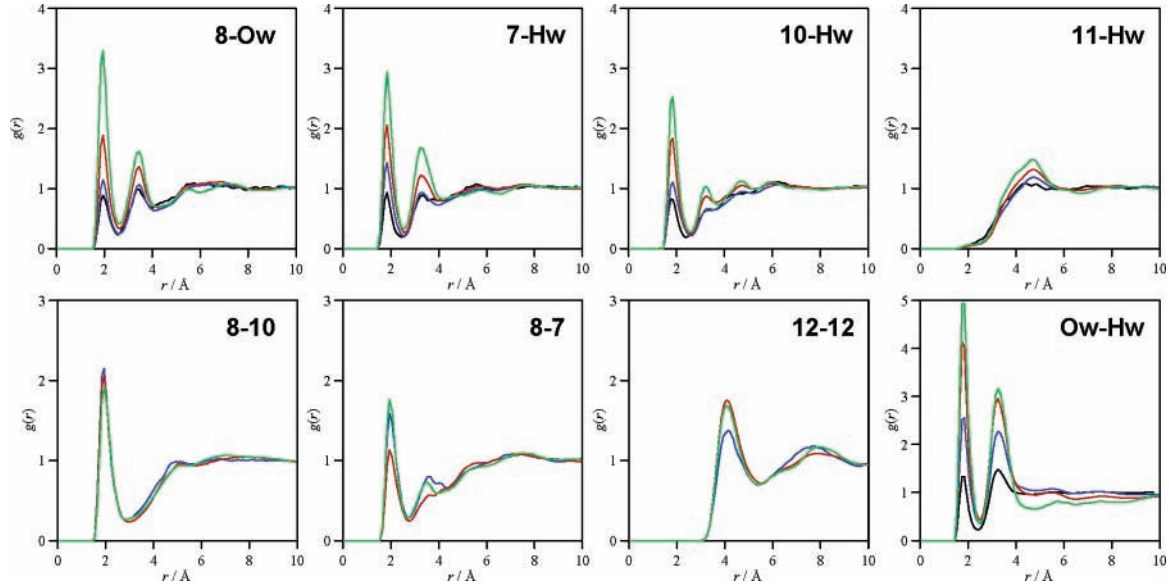

Figure 12. Site−site radial distribution functions, $g(r)$, for ML + water mixtures calculated from molecular dynamics simulations at different concentrations at 298 K and 0.1 MPa. (—) ML at infinite dilution ($x_{ML} = 0.004$); (blue) $x_{ML} = 0.25$; (red) $x_{ML} = 0.50$; and (green) $x_{ML} = 0.75$. x_{ML} = ML mol fraction. Atom numbering as in Figure 1; Ow and Hw are water oxygen and water hydrogen, respectively.

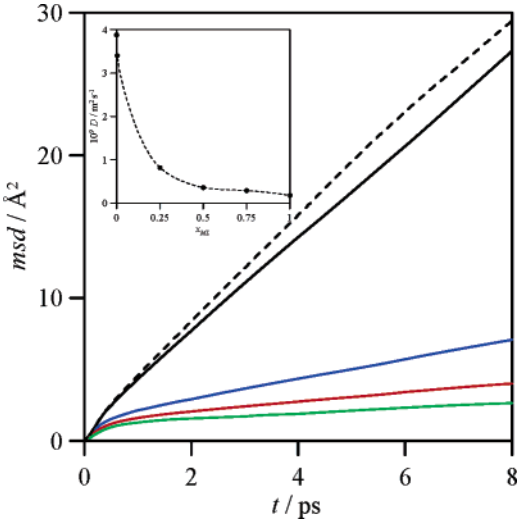

Figure 13. Mean square displacement, msd, and diffusion coefficient, D, for ML + water mixtures obtained from molecular dynamics simulations at 298 K and 0.1 MPa for different ML mol fractions, x_{ML}. Color as in Figure 12. (—) Pure SPC water. In inside plot: (●) D values obtained from calculated msd and (—) trend line.

several important pairs. An analysis of RDFs for 8−10, 8−7, and 8−11 pairs show that hydrogen bonding through the alkoxy oxygen is not produced, whereas remarkable hydrogen bonding through hydroxyl−hydroxyl and hydroxyl−carbonyl bonds is clearly present. The maxima in RDFs for 8−7 and 8−10 pairs appear at the same distance, 1.95 Å, but it is slightly stronger for the 8−10 interaction (2.84 for 8−10 and 1.83 for 8−7, at 298 K and 0.1 MPa), showing a slightly greater preference for the interaction through the carbonyl position, although hydrogen bonding in both positions will be present in the fluid. As the temperature increases, hydrogen bonding is weakened, both for 8−10 and 8−7 interactions, and a small shoulder appeared in the RDFs at short distances. The temperature effect on the 8−10 interaction is slightly lower than for the 8−7 pair (8−10 decreases by 33.8% and 8−7 by 39.3% on going from 298 to 373 K); thus, the 8−7 interaction is slightly weaker than the 8−10 one. The pressure effect on both interactions is very small, almost negligible for the 8−10 pair up to 50 MPa. A more

TABLE 4: Properties of ML + (Water or Methanol) and ML + Water + Methanol Mixtures for Different ML Mol Fractions, x_{ML}, Computed from Molecular Dynamics Simulations at 298 K and 0.1 MPa[a]

x_{ML}	ρ (g cm^{-3})	E_{int} (kcal mol^{-1})	c (MPa)	10^9 D (m^2 s^{-1})
		ML + water		
0	0.9899	−10.44	2404.77	3.88
0.004	0.9914	−10.47	2367.84	3.40
0.250	1.0686	−11.88	1344.23	0.82
0.500	1.0910	−13.20	987.20	0.36
0.750	1.0997	−14.51	808.74	0.29
		ML + methanol		
0	0.7780	−8.01	846.22	2.71
0.004	0.7811	−8.04	844.40	2.50
0.250	0.9260	−9.92	768.76	1.33
0.500	1.0128	−11.91	741.83	0.64
0.750	1.0670	−13.84	718.08	0.30
		0.333 ML + 0.333 water + 0.333 methanol		
	1.0126	−11.46	944.62	0.96

[a] Density, ρ; intermolecular energy, E_{int}; cohesive energy density, c (calculated ASC = $(-E_{int}/V_m)$); and diffusion coefficient, D (calculated from msd).

detailed analysis of RDFs for the 8−7 interaction shows the presence of small features at distances longer than the first sharp maxima, with a small peak at 3.55 Å, that are absent for the 8−10 pair; thus, for the hydroxyl−hydroxyl interactions, successive solvation shells are possible and provide a more cooperative bonding.

Another interesting fact to study is the methyl groups' arrangement in solution, to study the feasibility of apolar domains in the fluid. The RDFs for pairs involving both methyl groups are reported in Figure 9. The homo and hetero methyl pairs reported show remarkable maxima at 4.05 Å, slightly more intense for the 12−12 pair and for the hetero 1−12 pair. These RDFs point to the existence of an apolar domain within the ML liquid, probably permeating the structure arising from the hydrogen bonding interaction. This apolar aggregation is weakened as the temperature rises, because of the increasing molecular mobility, and reinforced with increasing pressure.

Another important feature to analyze is the prevailing ML conformation in solution. The results reported in the DFT section showed a clear preference for the ML1 conformer in the gas

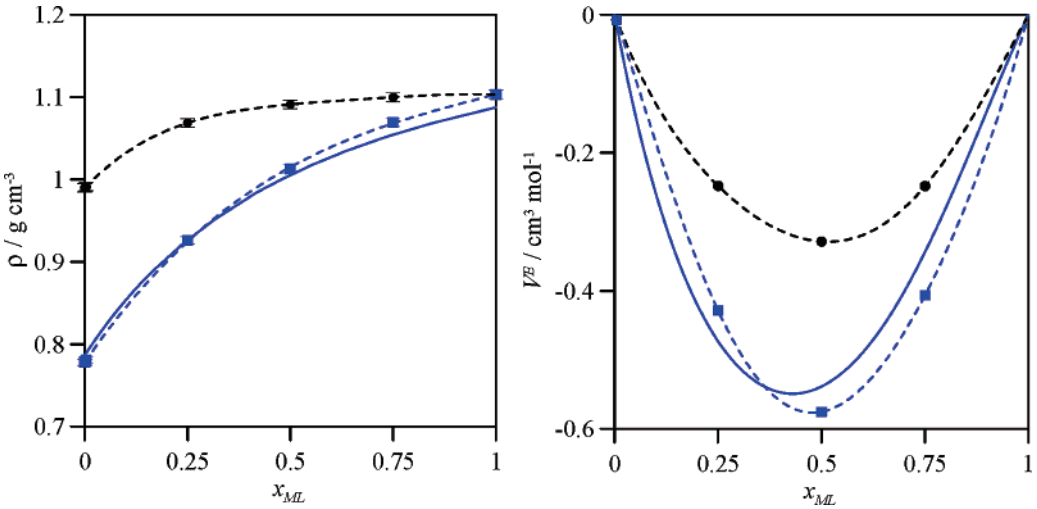

Figure 14. Density, ρ, and excess molar volume, V^E, for ML + (water or methanol) mixtures for different ML mol fractions, x_{ML}. (●,■) Computed results MD simulations, (---) trend lines from MD simulations, and (—, blue) experimental results from ref 37. Color code: (black) ML + water and (blue) ML + methanol.

phase that decreases on going to the water/methanol solution, but no results were reported for the effect on going to the ML solution. In Figure 10, the time evolution of the two important dihedral angles for the last 100 ps of the simulations is reported for different temperatures and pressures, and the results show how in solution the (7−5−9−10) dihedral angle is around 60°, with very mild temperature and pressure effects, whereas the (8−7−5−9) angle is close to zero. Thus, the hydroxyl group is not in plane with the carbonyl group, but the hydroxyl hydrogen is pointing toward the carbonyl group; hence, although the intermolecular hydrogen bonding is weakened, it is also possible to establish this interaction, giving rise to an intermediate situation among the aforementioned DFT results for the gas phase and water/methanol solution. A deformed ML1 conformed seems to be the prevailing one in lactate solutions.

To confirm the existence of apolar (formed by methyl groups)/polar (established through hydrogen bonding networks) domains, a representative average snapshot of fluid ML is reported in Figure 1 (Supporting Information). The color code used distinguishes among the apolar (green) and polar (red) zones; in this picture, continuous regions of both domains appear to be permeating each other, giving rise to a highly structured fluid.

The dynamic properties of liquid ML were also analyzed according to the time evolution of the mean square displacement (msd) (Figure 11) and from the diffusion coefficients (Table 3). The diffusion coefficients, D, were calculated according to Einstein's relation

$$D = \frac{1}{6}\lim_{t\to\infty}\langle \Delta r(t)^2 \rangle \qquad (3)$$

where the quantity in brackets, msd, is plotted in Figure 11 for the first 8 ps of the simulation at the studied temperatures and pressures. Diffusion coefficients were calculated from the msd slopes once the linear regime was reached. The msd increases, and so does D, with increasing temperature and decreases with increasing pressure as we may expect. Low diffusion coefficients are obtained for ML; for instance, it is an order of magnitude lower than those for pure water, pointing to a fluid highly structured through hydrogen bonding in which the molecular mobility is low.

Finally, molecular dynamics simulations were used to predict several important properties for ML (Table 3). These properties are frequently required in many stages of process design, in which an accurate experimental measurement as a function of pressure and temperature is not always feasible because of technical, economical, and/or time constraints; thus, theoretical predictions are very valuable. On the other side, comparison of predicted properties with experimental ones allows us to test the accuracy of the molecular model underlying the simulations and then of the molecular level conclusions inferred from the simulations. Accurate thermophysical experimental data for ML are very scarce in the literature, and no data could be found at high temperatures/high pressures. Density predictions are slightly greater than the experimental ones (1.2 or 1.4% depending of the literature source (Table 3)), but deviations are remarkably low. Intermolecular energies show a fluid with strong intermolecular interactions; thus, although DFT results showed that intermolecular forces were weakened on going to solution, liquid ML is a fluid that is highly structured. The cohesive energy density, c, reported in Table 3 allows the calculation of Hildebrand solubility parameters ($\delta = c^{1/2}$), which are very important for solubility applications and whose determination as a function of pressure/temperature is very difficult; the calculated c values are characteristic of hydrogen bonded fluids.

3.2.2. ML + Water Binary Mixtures. Molecular dynamics simulations for ML + water binary mixtures were carried out at 298 K, 0.1 MPa for 0.004 (high dilution, only ML/water interactions), 0.25, 0.50, and 0.75 ML mol fractions. RDFs for several selected homo- and heteromolecular pairs are reported in Figure 12. The interaction among water and ML molecules could be established through the carbonyl or alkoxy oxygens and through the hydroxyl group, and the reported RDFs show that interaction in the alkoxy position, 11-Hw, is not developed in solution. The interaction in the carbonyl oxygen is slightly less intense than the one through the hydroxyl group, and the interaction in both sites is surprisingly reinforced as the ML concentration increases. This shows that at low ML concentrations, the effect of ML on the water hydrogen bonding network is very subtle, as is shown by the Ow-Hw RDFs, but when the ML mol fraction increases, strong interactions with water are established, which also reinforce the water network. RDFs reported for 8-Ow, 7-Hw, and 10-Hw pairs show a second sharp peak whose intensity also increases with ML concentration; thus, a second solvation shell is developed around ML molecules, and a detailed analysis of RDFs at longer distances shows a

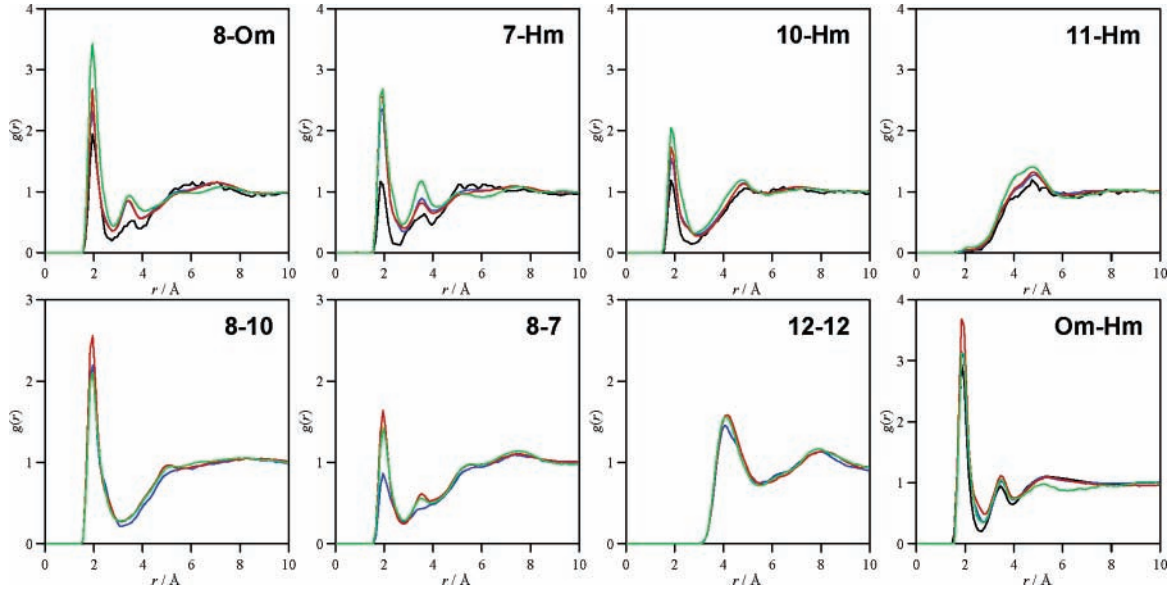

Figure 15. Site−site radial distribution functions, $g(r)$, for ML + methanol mixtures calculated from molecular dynamics simulations at different concentrations at 298 K and 0.1 MPa. ML at infinite dilution ($x_{ML} = 0.004$) (black); $x_{ML} = 0.25$ (blue); $x_{ML} = 0.50$ (red); and $x_{ML} = 0.75$ (green). x_{ML} = ML mol fraction. Atom numbering as in Figure 1; Om and Hm are methanol oxygen and hydrogen bonded to oxygen, respectively.

third and probably a fourth shell. Hence, water is highly structured around ML. These water/ML heteroassociations only slightly decrease the ML/ML interactions, as we may conclude if the RDFs for the 8−10 and 8−7 pairs in Figures 9 and 12 are compared and if the apolar domain across the fluid, RDFs for the 12−12 pair, is reinforced with increasing ML concentration. Thus, when water and ML are mixed, hydrogen bonding networks of both fluids permeate and reinforce, giving rise to remarkable heteroassociations more efficient as the ML concentration increases.

The dynamic properties for this binary system are reported in Figure 13 and Table 4. The msd for the first 8 s of the simulations reported in Figure 13 shows how the addition of ML to water decreases the molecular mobility of the mixed fluid. The computed msd for SPC water is also reported as well as the *D* value in Table 4 for control purposes, and this value is in agreement with literature values for this water model.[29a] The lower mobility is produced by the heteroassociation effect on the fluid dynamics by the reinforcement of the hydrogen bonding mixed networks.

Several computed thermophysical properties for this mixed fluid are also included in Table 4. The reported properties show a denser fluid as the ML concentration increases with increasing interaction energy and decreasing cohesive energy density. Computed density and derived excess molar volume are reported in Figure 14, and although no experimental data are available for this system, the remarkable deviations from ideality are in agreement with literature negative excess enthalpy data that also point to strong heteroassociations.[38] The computed excess volume shows a very efficient packing in the mixture, confirming the permeation of water and ML hydrogen bonding networks.

3.2.3. ML + Methanol Binary Mixtures. The behavior of this system is very similar to the one containing water. Interaction among methanol and ML molecules is established through the carbonyl oxygen and hydroxyl positions and discarded for the alkoxy site. The interaction in the hydroxyl site is very strong even for very low ML concentrations, comparing RDFs for 8-Ow and 8-Om in Figures 12 and 15. Although a second maximum also appears in RDFs involving hydroxyl groups for methanol solutions, it is less intense and

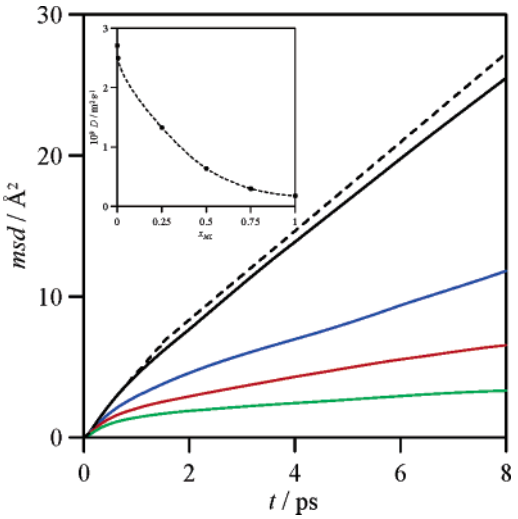

Figure 16. Mean square displacement, msd, and diffusion coefficient, *D*, for ML + methanol mixtures obtained from molecular dynamics simulations at 298 K and 0.1 MPa for different ML mol fractions, x_{ML}. Color as in Figure 15. In inside plot: (●) *D* values obtained from calculated msd and (—) trend line.

sharp than for water solutions, pointing to worse solvation in the second and consecutive shells probably because of the bigger size of the methanol molecules. The interaction among ML molecules also remains in methanol solutions and is almost unaffected by ML concentration as it happens for apolar methyl domains. Methanol molecules are also strongly hydrogen bonded (see Om-Hm RDFs), but the effect of ML on this interaction is very small if compared with water solutions; thus, the methanol structure is not so efficiently reinforced by the presence of ML molecules. The addition of ML molecules has a remarkable effect on msd (Figure 16), although this effect is less intense than in water solutions (compare Figures 13 and 16). For instance, on going from pure water to a 0.004 ML solution, a decrease of 12.4% is produced in *D*, whereas for the same conditions, only a 7.8% decrease is produced for methanol. Hence, effective inter- and intramolecular hydrogen bonding is produced in methanol/ML solutions, although this is less intense than in water solutions.

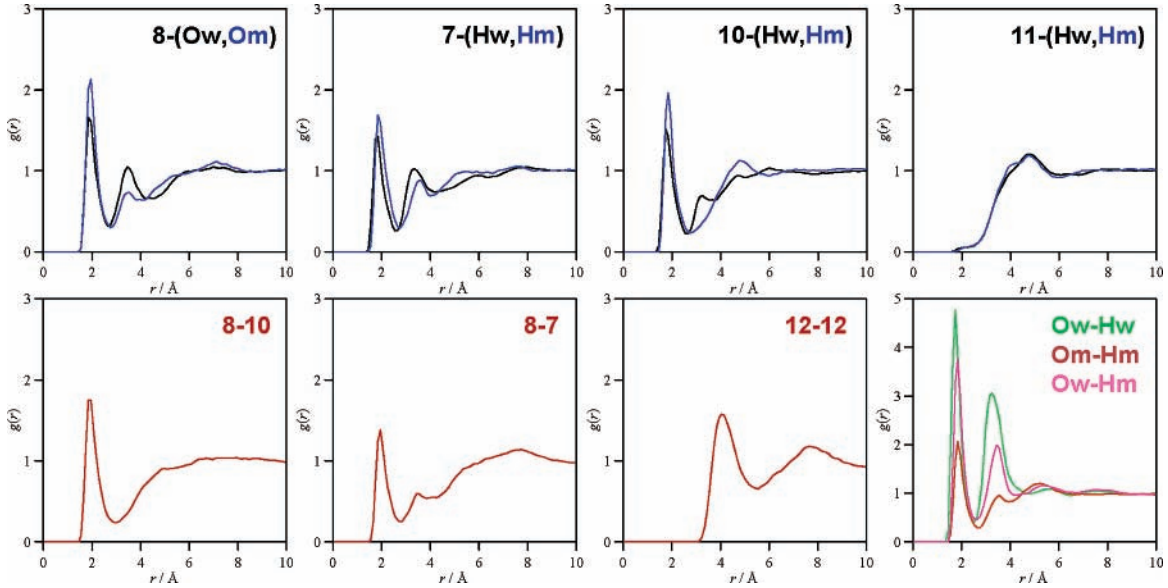

Figure 17. Site−site radial distribution functions, $g(r)$, for 0.333 ML + 0.333 water + 0.333 methanol mixture calculated from molecular dynamics simulations at 298 K and 0.1 MPa. ML atom numbering as in Figure 1; Ow and Hw = water oxygen and hydrogen and Om and Hm = methanol oxygen and hydrogen bonded to oxygen.

Computed thermophysical properties for this binary system are reported in Table 4, and interaction energies and cohesive energy densities are lower than in water solutions, confirming the aforementioned weaker interactions. Density values increase remarkably with ML concentration and are in excellent agreement with experimental values (Figure 14), with greater deviations in the vicinity of pure ML but always being around 1%. This level of agreement should be considered to be very good because computations are purely predictive, and none of the parameters used in the simulations was adjusted to match any experimental data. Computed excess molar volumes are also in agreement with experimental ones in a qualitative and quantitative way, showing the accuracy and reliability of the molecular model used in the simulations. An excess volume reflects deviations from ideality, and it is the result of a very delicate balance of effects arising from geometric and intermolecular force factors that are usually very difficult to describe accurately from a purely theoretical model. The excess molar volume is remarkably negative and lower than for water/ML mixtures because packing in pure methanol is less effective than in pure water. The permeation of methanol and ML networks with the new heteroassociations arising among both molecules produces a very efficient packing as it shown by the compression upon mixing. Thus, the high nonideality of this system, as that for ML/water, is correctly captured by the simulations reported.

3.2.4. ML + Water + Methanol Ternary Mixture. To analyze the effect of the simultaneous presence of the three studied molecules on the mixed fluid structure, the ternary mixture 0.333 ML + 0.333 water + 0.333 methanol was simulated at 298 K and 0.1 MPa, where the numbers show the mol fraction of each compound.

RDFs for several selected pairs are reported in Figure 17. From this figure, we may conclude that the interaction among ML and water/methanol molecules is established only through the hydroxyl and carbonyl oxygens of the ester molecule as for binary systems. RDFs are very similar for both ML sites, either for water and methanol sites, and thus, ML interacts with both molecules simultaneously through the carbonyl oxygen and hydroxyl group. RDFs are slightly more intense for methanol/ML pairs, and thus, a weak preferential solvation by the alcohol molecules in the ML solvation spheres is established. Strong hydrogen bonding is established with both molecules. The interaction among ML molecules remains in this complex mixture as RDFs for 8−10 and 8−7, although this is weakened as compared with pure ML (see Figure 9). There is a slight preference for the interaction involving hydroxyl and carbonyl pairs than involving only hydroxyl pairs; RDFs for the 8−10 pair is slightly greater than for 8−7 pair, although hydrogen bonding is established in both ways. RDFs for methyl groups show remarkable peaks at 4 Å, pointing to the existence of apolar domains even in this complex ternary mixture. Finally, RDFs for homo pairs for water and methanol molecules show how these molecules continue strongly interacting among them in this mixture. We should remark on the strong reinforcement of water interactions deduced from the very large first peak in Ow-Hw RDF. Water−methanol strong interactions are also established; thus, in the solvation spheres around ML, a complex hydrogen bonding network is established in which water−water, methanol−methanol, and water−methanol are developed at the same time that both molecules interact remarkably with the ester molecules.

Thermophysical properties for this ternary mixture are reported in Table 4. No experimental data are available to carry out comparisons; however, the high values of intermolecular energy and cohesive density energy are a consequence of the strong hydrogen bonding. This is confirmed also by the low diffusion constant of the mixture closer to that of ML than of the water/methanol ones.

4. Conclusion

The properties and structure of ML in the gas phase and water/methanol solutions are analyzed from DFT and molecular dynamics simulations. In the gas phase conformer, allowing intramolecular hydrogen bonding among hydroxyl and carbonyl hydrogen bonding is clearly preferred, but on going to solution, a greater molecular flexibility is obtained because of the lower corresponding torsional barriers. Clusters by self-association among ML molecules are stable in the gas phase, but the binding energy decreases remarkably in the liquid phase. In ML/water or methanol binary mixtures, a very complex structure is obtained in which hydrogen bonding is established among

molecules of different types, a very effective solvation is established around ML molecules, and a slightly more effective solvation occurs in water solutions, and this gives rise to the reinforcement of the hydrogen bonding networks. In ternary ML/water/methanol mixtures, a mixed solvation sphere is developed in which the hydrogen bonding is established among all the possible sites, and a slightly preferential solvation by methanol molecules could be deduced. Hence, highly structured fluids are obtained from the simulations, both for pure ML as well as for their mixtures with water and methanol, in which complex hydrogen bonding networks determine the fluid properties.

The predicted thermophysical properties are in excellent agreement with the available experimental ones that on one hand validate the results reported in this work and on the other hand allow the reliable simulation of these properties at other temperatures/pressures for which no experimental data are available.

Supporting Information Available: Molecular parameters for the lower energy conformations of methyl lactate calculated at the B3LYP/6-311++g** theoretical level in the gas phase and water and methanol solutions (Table S1) and snapshot of average liquid structure of ML obtained from molecular dynamics simulations (Figure 1). This material is available free of charge via the Internet at http://pubs.acs.org.

References and Notes

(1) Anastas, P.; Warner, J. *Green Chemistry Theory and Practice*; Oxford University Press: Cambridge, 1998.

(2) Meyer, H. *J. Bus. Strat*. **2000**, *21*, 38.

(3) Nameroff, T. J.; Garant, R. J.; Albert, M. B. *Res. Policy* **2004**, *33*, 959.

(4) DeSimone, J. *Science* **2002**, *297*, 799.

(5) Bhattacharya, A.; Purohit, V. C. *Org. Process Res. Dev*. **2003**, *7*, 254.

(6) Sheldon, R. A. *Green Chem*. **2005**, *7*, 267.

(7) (a) Bowner, C. T.; Hooftman, R. N.; Hanstveit, A. O.; Venderbosch van der Hoewen, N. *Chemosphere* **1998**, *7*, 1317. (b) Clary, J. J.; Feron, V. J.; Van Velthuijsen, J. A. *Regul. Toxicol. Pharmacol*. **1998**, *27*, 88. (c) Cosmetic Ingredient Review Expert Panel. *Int. J. Toxicol*. **1998**, *17* (Suppl. 1), 1−243.

(8) Vu, D. T.; Lira, C. T.; Navichandra, S. A.; Kolah, A. K.; Miller, D. *J. Chem. Eng. Data* **2006**, *51*, 1220.

(9) (a) Asthana, N.; Kolah, A. K.; Vu, D. T.; Lira, C. T.; Miller, D. *Org. Process Res. Dev*. **2005**, *9*, 959. (b) Benedict, D. J.; Parulekar, S. J.; Tsai, S. P. *Ind. Eng. Chem. Res.* **2003**, *42*, 2282. (c) Datta, R.; Tsai, S. P. U.S. Patent 5,723,639, 1998.

(10) (a) Nikles, S. M.; Piao, M.; Lane, A. M.; Nikles, D. E. *Green Chem*. **2001**, *3*, 109. (b) Tychta, K.; Sandberg, D. A.; Henry, M.; Datta, R. *Evaluation of Environmentally Benign Green Solvent Versol Ethyl Lactate for Machine Shop Parts Cleaning and Degreasing*; Pilot Project Report for Argonne National Laboratory: Argonne, IL, 1999. (c) Datta, R.; Henry, M.; Tsai, S. P.; Halpen, Y.; Frank, J. R. Proceedings from the 3rd Annual Green Chemistry Engineering Conference; Washington, DC, 1999.

(11) (a) Dohrn, R.; Pfohl, O. *Fluid Phase Equilib*. **2002**, *15*, 194−197. (b) Marcus, Y. *The Properties of Solvents*; Wiley: New York, 1998.

(12) (a) Sanz, M. T.; Murga, R.; Beltrán, S.; Cabezas, J. L.; Coca, J. *Ind. Eng. Chem. Res*. **2002**, *41*, 512. (b) Sanz, M. T.; Beltrán, S.; Calvo, J. L.; Cabezas, J. L.; Coca, J. *Chem. Eng. Data* **2003**, *48*, 1446.

(13) Frisch, M. J.; Trucks, G. W.; Schlegel, H. B.; Scuseria, G. E.; Robb, M. A.; Cheeseman, J. R.; Montgomery, J. A., Jr.; Vreven, T.; Kudin, K. N.; Burant, J. C.; Millam, J. M.; Iyengar, S. S.; Tomasi, J.; Barone, V.; Mennucci, B.; Cossi, M.; Scalmani, G.; Rega, N.; Petersson, G. A.; Nakatsuji, H.; Hada, M.; Ehara, M.; Toyota, K.; Fukuda, R.; Hasegawa, J.; Ishida, M.; Nakajima, T.; Honda, Y.; Kitao, O.; Nakai, H.; Klene, M.; Li, X.; Knox, J. E.; Hratchian, H. P.; Cross, J. B.; Adamo, C.; Jaramillo, J.; Gomperts, R.; Stratmann, R. E.; Yazyev, O.; Austin, A. J.; Cammi, R.; Pomelli, C.; Ochterski, J. W.; Ayala, P. Y.; Morokuma, K.; Voth, G. A.; Salvador, P.; Dannenberg, J. J.; Zakrzewski, V. G.; Dapprich, S.; Daniels, A. D.; Strain, M. C.; Farkas, O.; Malick, D. K.; Rabuck, A. D.; Raghavachari, K.; Foresman, J. B.; Ortiz, J. V.; Cui, Q.; Baboul, A. G.; Clifford, S.; Cioslowski, J.; Stefanov, B. B.; Liu, G.; Liashenko, A.; Piskorz, P.; Komaromi, I.; Martin, R. L.; Fox, D. J.; Keith, T.; Al-Laham, M. A.; Peng, C. Y.; Nanayakkara, A.; Challacombe, M.; Gill, P. M. W.; Johnson, B.; Chen, W.; Wong, M. W.; Gonzalez, C.; Pople, J. A. *Gaussian 03*, Revision C.02; Gaussian, Inc.: Pittsburgh, PA, 2004.

(14) Becke, A. D. *Phys. Rev. A* **1988**, *38*, 3098.

(15) Lee, C.; Yang, W.; Parr, R. G. *Phys. Rev. B* **1988**, *37*, 785.

(16) Becke, A. D. *J. Chem. Phys*. **1993**, *98*, 5648.

(17) Singh, U. C.; Kollman, P. A. *J. Comput. Chem.* **1984**, *5*, 129.

(18) (a) Besler, B. H.; Merz, K. M.; Kollman, P. A. *J. Comput. Chem.* **1990**, *11*, 431. (b) Martin, F.; Zipse, H. *J. Comput. Chem*. **2005**, *26*, 97. (c) Sigfridsson, E.; Ryde, U. *J. Comput. Chem*. **1998**, *19*, 377. (d) Wong, C. Y.; Sony, J.; Aluru, N. R. *J. Chem. Phys*. **2006**, *125*, 114701. (e) Morrow, T. I.; Maginn, E. *J. Phys. Chem. B* **2002**, *106*, 12807. (f) Chelli, R.; Procacci, P.; Cardini, G.; Della Valle, R. G.; Califano, S. *Phys. Chem. Chem. Phys*. **1999**, *1*, 871.

(19) Cances, E.; Mennucci, B. *J. Math. Chem*. **1998**, *23*, 309.

(20) (a) Boys, S. F.; Bernardu, F. *Mol. Phys*. **1970**, *19*, 553. (b) Simon, S.; Duran, M.; Dannenberg, J. J. *J. Chem. Phys.* **1996**, *105*, 11024.

(21) Ponder, J. W. *TINKER: Software Tool for Molecular Design*, 4.2 ed.; Washington University School of Medicine: St. Louis, MO, 2004.

(22) Hoover, W. G. *Phys. Rev. A* **1985**, *31*, 1695.

(23) Allen, M. P.; Tildesley, D. J. *Computer Simulation of Liquids*; Clarendon Press: Oxford, 1989.

(24) Essmann, U. L.; Perera, M. L.; Berkowitz, T.; Darden, H.; Lee, H.; Pedersen, L. G. *J. Chem. Phys*. **1995**, *103*, 8577.

(25) Martínez, J. M.; Martínez, L. *J. Comput. Chem*. **2003**, *24*, 819.

(26) Jorgensen, W. L.; Maxwell, D. S.; Tirado-Rives, J. *J. Am. Chem. Soc*. **1996**, *118*, 11225.

(27) (a) Rizzo, R. C.; Jorgensen, W. L. *J. Am. Chem. Soc*. **1999**, *121*, 4827. (b) McDonald, N. A.; Jorgensen, W. L. *J. Phys. Chem. B* **1998**, *102*, 8049. (c) Kaminski, G.; Duffy, E. M.; Matsui, T.; Jorgensen, W. L. *J. Phys. Chem.* **1994**, *98*, 13077.

(28) (a) Berendsen, H. J. C.; Postman, J. P. M.; van Gunsteren, W. F.; Hermans, J. In *Intermolecular Forces*; Pullman, B., Ed.; Reidel: Dordrecht, The Netherlands, 1981. (b) Berweger, C. D.; van Gunsteren, W. F.; Müller-Plathe, F. *Chem. Phys. Lett*. **1995**, *232*, 429.

(29) (a) Mahoney, M. W.; Jorgensen, W. L. *J. Chem. Phys.* **2001**, 114, 363. (b) Mark, P.; Nilsson, L. *J. Phys. Chem. A* **2001**, *105*, 9954. (c) de Pablo, J.; Prausnitz, J. M.; Strauch, H. J.; Cummings, P. T. *J. Chem. Phys*. **1990**, *93*, 7355. (d) Jorgensen, W. L.; Chandrasekhar, J.; Madura, J. D.; Impey, R. W.; Klein, M. L. *J. Chem. Phys*. **1983**, *79*, 926. (e) Guedes, R. C.; Countinho, K.; Costa Cabral, B. J.; Canuto, S. *J. Phys. Chem. B* **2003**, *107*, 4304.

(30) Gigante, D. M. P.; Long, F. L.; Bodack, L. A.; Evans, J. M.; Kallmerten, J.; Nafie, L. A.; Freedman, T. B. *J. Phys. Chem. A* **1999**, *103*, 1523.

(31) Borba, A.; Gómez-Zavaglia, A.; Lapinski, L.; Fausto, R. *Vib. Spectrosc*. **2004**, *36*, 79.

(32) Borho, N.; Suhn, M. A. *Org. Biomol. Chem.* **2003**, *1*, 4351.

(33) Farnik, M.; Weimann, M.; Steinbach, C.; Buck, U.; Borho, N.; Adler, T.; Suhm, M. A. *Phys. Chem. Chem. Phys.* **2006**, *8*, 1148.

(34) Adler, T. B.; Borho, N.; Reiher, M.; Suhm, M. A. *Angew. Chem., Int. Ed*. **2006**, *45*, 3440.

(35) Borho, N.; Suhn, M. A.; Le Barbu-Debus, K.; Zechnacker, A. *Phys. Chem. Chem. Phys.* **2006**, *8*, 4449.

(36) Kimura, T.; Ozaki, T.; Takagi, S. *Chirality* **1998**, *10*, 722.

(37) Sanz, M. T.; Calvo, B.; Beltrán, B.; Cabezas, J. L. *J. Chem. Eng. Data* **2002**, *47*, 1003.

(38) Sanz, M. T.; Gmehling, J. *J. Chem. Eng. Data* **2005**, *50*, 85.